JOURNAL OF GUIDANCE, CONTROL, AND DYNAMICS
Vol. 19, No. 5, September–October 1996

Quantitative Feedback Theory with a Scheduled Gain for Full Envelope Longitudinal Control

S. Antony Snell* and Perry W. Stout†
University of California at Davis, Davis, California 95616

Two approaches to control law design for the unstable, nonlinear, short-period dynamics of the F-16 aircraft using nonlinear quantitative feedback theory (QFT) are presented. The first is a conventional QFT design, whereas the second uses a variable gain before applying QFT. Large uncertainty templates result from using a set of linear time invariant equivalent models to accurately represent the nonlinear aircraft dynamics over a wide operating envelope. It is shown that including the variable gain, which is inversely proportional to speed, has the beneficial effect of reducing the size of these templates. Once the modified templates have been obtained, the traditional QFT method is applied to yield a controller, which meets the same performance criteria, while using lower control effort. The gain-scheduled QFT controller is endowed with the usual, good robustness qualities of QFT designs while requiring lower gain at high speeds than the fixed-gain controller. The reduced gain provides improved phase margin and eliminates a tendancy for excessive elevator and pitch rate oscillations at high speed.

Nomenclature

$C_{M_\alpha}, C_{M_q}, C_{M_{\delta e}}$	= nondimensional partial derivative of C_M with respect to α, q, δ_e
C_X, C_Z, C_M	= nondimensional coefficient of x/z force/pitching moment
$\bar{c}$	= mean aerodynamic chord
I_{yy}	= moment of inertia about pitch axis
M	= aerodynamic pitching moment
m	= mass
q	= pitch rate, $\dot{\theta}$
$\bar{q}$	= dynamic pressure, $\frac{1}{2}\rho V^2$
S	= swept area of wings
u, w	= body x, z components of velocity
V	= magnitude of velocity
X, Z	= aerodynamic force in body x, z direction
α	= angle of attack, $\tan^{-1}(w/u)$
δ_e	= elevator deflection
θ	= pitch attitude angle

I. Introduction

THERE has been increasing interest in poststall flight recently, and now several aircraft have some level of poststall capability, including the F-16 AFTI, F-18 HARV, X-29, F-22, and X-31. References 1 and 2 demonstrate that the poststall capabilities of the X-31 provide a decisive advantage in close-in combat over aircraft not possessing such capabilities.

The design of flight control laws for poststall flight is challenging because the prevailing dynamics are nonlinear and uncertain. The nonlinearities arise from both the aerodynamics and the inertial coupling terms. Figure 1 illustrates that C_M for the F-16 is a highly nonlinear function of angle of attack (AOA) and δ_e when AOA exceeds 35 deg. The conventional approach to control law synthesis is to schedule the controller gains as functions of slowly varying parameters such as V and even with AOA. However, Ref. 3 states that gain scheduling with respect to a rapidly changing variable such as AOA can often lead to stability problems. Furthermore, designing the schedules is usually laborious and time consuming.

One alternative to gain scheduling is dynamic inversion,[4,5] which uses control inputs to directly cancel unwanted terms in the nonlinear state equations and replace them with desirable dynamics. Dynamic inversion applies directly to nonlinear systems without the need for multiple linearized models required for gain scheduling. References 6–8 examine the robustness of dynamic inversion flight control; it appears quite robust to static variations in aerodynamic force and moment coefficients. However, this robustness is sometimes obtained by using high loop gains, which may prove detrimental in the presence of unmodeled dynamics and sensor noise.

A third approach is to design a single, linear controller with sufficient robustness to provide good performance in the presence of the large variations in aircraft dynamics encountered during poststall flight. The potential drawback of using a single, linear controller design is that it may be overly conservative since it must be robust to such large variations. The advantage is that powerful tools exist to design robust, linear control laws, notably μ-synthesis and quantitative feedback theory (QFT). Although μ synthesis has a rigorous mathematical background, it is not obvious to many in its workings. In contrast, QFT[9–11] provides a fairly transparent path to robust control design for the single-input/single-output (SISO) case.

QFT has been used to design flight control laws. In Refs. 12 and 13 a multi-input/multi-output (MIMO) control law for a helicopter operating over a wide flight envelope is designed, whereas Reynolds et al.[14] apply QFT to a highly maneuverable combat aircraft. One of the shortcomings has been that the wide variation in

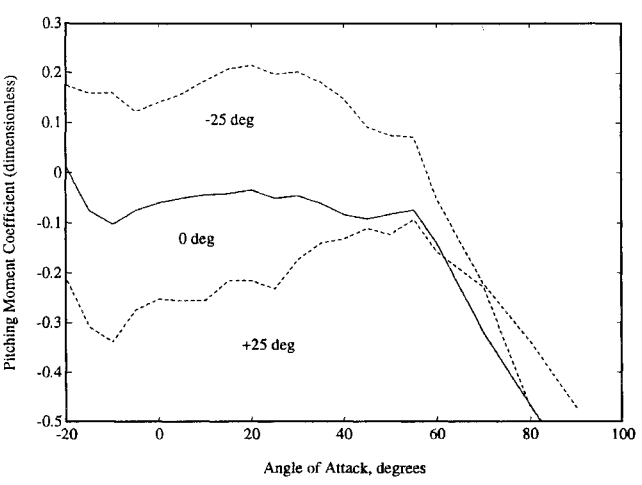

Fig. 1 F-16 pitching moment coefficient C_m as function of α and δ_e.

Presented as Paper 95-3254 at the AIAA Guidence, Navigation, and Control Conference, Baltimore, MD, Aug. 7–10, 1995; received Sept. 28, 1995; revision received May 7, 1996; accepted for publication May 9, 1996.

*Assistant Professor, Mechanical and Aeronautical Engineering. Senior Member AIAA.

†Graduate Student, Mechanical and Aeronautical Engineering. Senior Member AIAA.

aircraft dynamics often require undesirably high loop gain to maintain performance over the entire envelope. To address this problem, Horowitz[15] proposes a nonlinear cancellation scheme similar to dynamic inversion to precondition the nonlinear dynamics into a linear form before applying QFT. The resulting system permits loop gain to be considerably reduced.

Two approaches are examined. The first approach, discussed in Secs. IV and V, uses a single, linear compensator designed to control AOA over the whole operating envelope. The design technique is an extension of QFT to nonlinear systems.[10] A nonlinear mathematical model of the unstable, short-period dynamics of the F-16 aircraft is constructed, then the nonlinear dynamics are represented by a set of linear time invariant equivalent (LTIE) models. These models are used to form uncertainty templates in the traditional QFT fashion and then a controller is designed meeting the requisite performance and robustness criteria. The second approach, referred to as gain scheduled, is presented in Secs. VI and VII. It is a hybrid combining QFT with a single variable gain, placed in series between the controller and plant. This gain is proportional to $1/V$ and is used to partly compensate for variation in elevator control effectiveness, which is proportional to $\bar{q} = \frac{1}{2}\rho V^2$. As a result, the sizes of some uncertainty templates are reduced, leading to a less conservative controller design. This is a simpler alternative to the full nonlinear cancellation of Ref. 15.

The remainder of this paper is as follows. Section II briefly describes the QFT methodology. Section III discusses the F-16 model used to conduct simulations. Sections IV–VII present specifics of the two control laws and simulation results. Conclusions are given in Sec. VIII.

II. Quantitative Feedback Theory

Horowitz[9] originally devised QFT to design controllers for highly uncertain, linear time invariant, SISO systems. However, Refs. 10–14 demonstrate extensions of QFT to MIMO, nonlinear and time varying plants.

The objective of QFT is to select the two transfer functions $C(s)$ and $F(s)$, shown in Fig. 2, to ensure that the output $\alpha(t)$ in response to input $\alpha_{\text{stick}}(t)$ falls within the set of acceptable responses $\mathcal{A}$ for any plant in the class $\mathcal{P}$. Here $\mathcal{P}$ is the set of all possible models representing the aircraft dynamics. Determining the extent of $\mathcal{P}$ is discussed in Sec. IV, whereas $\mathcal{A}$ is defined in terms of desired time responses to given inputs. These time domain specifications are converted to a specification on the closed-loop transfer function by dividing the Laplace transforms of $\alpha(t)$ signals in $\mathcal{A}$ by the Laplace transform of the corresponding input signal $\alpha_{\text{stick}}(t)$.

QFT designs are created on the Nichols chart: a plot of phase as abscissa and log magnitude as ordinate, both parameterized by frequency ω. Because a whole set of plants $\mathcal{P}$ rather than a single plant P is considered during the QFT design, the magnitude and phase of $\mathcal{P}$ at each frequency yields a set of points on the Nichols chart instead of a single point. Thus, at each selected frequency a connected region or template $\boldsymbol{P}$ is constructed, which encloses this set of points. Larger templates indicate greater uncertainty and so, to avoid unnecessary conservatism, the template is usually chosen to be the smallest, convex polygon enclosing all of the points.

To make a Nichols chart of $P(j\omega)C(j\omega)$, the phases of $C(j\omega)$ and $P(j\omega)$ are added to get the new abscissa, and the log magnitudes of $C(j\omega)$ and $P(j\omega)$ are added to find the new ordinate. Thus, multiplying $P(j\omega)$ by $C(j\omega)$ simply translates points on the Nichols chart. By extension the compensated template $\boldsymbol{PC}(j\omega)$ is obtained by simply translating the template $\boldsymbol{P}$ on the Nichols chart. The size, shape, and orientation of $\boldsymbol{P}$ do not change.

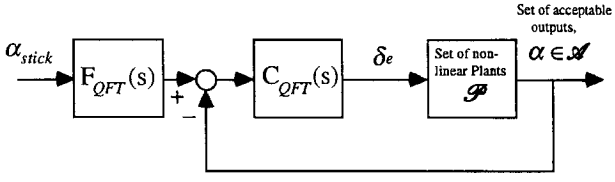

Fig. 2 QFT control configuration.

M curves, contours of constant closed-loop magnitude, are also plotted on the Nichols chart. The M curves become less dense above and to the right of the critical -1 point with unity magnitude and -180-deg phase, indicating that the closed-loop magnitude is less sensitive to gain and phase variations in this area of the chart than in regions closer to the -1 point. Typically, $C(j\omega)$ is chosen to push low-frequency templates into this area because the specifications on the closed-loop transfer functions are tighter at low frequency. The cost of this movement is that $C(j\omega)$ must provide increased gain. An ideal QFT design for $C(j\omega)$ moves each template just high enough to fit between any two M curves corresponding to a difference in closed-loop magnitude that meets the design specification. Moving the template higher on the chart requires higher gain within the loop, which can be damaging in terms of unmodeled dynamics and actuator usage caused by sensor noise, especially at higher frequencies. Notice that only the variation in closed-loop magnitude is considered when designing $C(j\omega)$, the absolute magnitude of the closed-loop transfer function is not important because the final, closed-loop transfer function is reshaped to meet the absolute magnitude specifications using the prefilter $F(s)$.

The preceding description of QFT applies to linear plants. Reference 10 extends QFT to nonlinear systems by substituting the LTIE system that most closely reproduces the response of the nonlinear system to a given input. Because of the nonlinearity, there is usually a different LTIE model for each input and initial condition considered. These LTIE models constitute the set of all possible plants $\mathcal{P}$. After substituting the set of LTIE models for the nonlinear system, the design of $C(s)$ and $F(s)$ is basically as already described. Because the specific LTIE model that best approximates the nonlinear dynamics in any given maneuver is included in $\mathcal{P}$, the closed-loop response of the nonlinear system in that maneuver must also be acceptable. This approach can be rather conservative because the variation in dynamic response caused by nonlinearity often yields large templates. Thus, although the response of the aircraft in a given maneuver may be accurately known, it is assumed to be uncertain and may be that of any LTIE model in the set $\mathcal{P}$. In Sec. VI it is shown that placing a V-dependent gain G_V in series with the plant reduces the nonlinear effect of speed on the dynamics. This reduces the heights of some uncertainty templates allowing lower gain to be used in $C(s)$. When the design of $C(s)$ is complete, G_V is subsumed into the compensator $G_V C(s)$.

III. F-16 Model

Nguyen et al.[16] contains data for a six-degree-of-freedom, nonlinear, rigid-body model of the F-16 aircraft, including tabular aerodynamic data of force and moment coefficients for AOA from -20 to $+90$ deg. The model used here is a simplified, short-period model based on that data and so only requires the longitudinal state equations (1a–1d):

$$\dot{u} + qw = \frac{T + X}{m} - g\sin\theta \tag{1a}$$

$$\dot{w} - qu = \frac{Z}{m} + g\cos\theta \tag{1b}$$

$$\dot{q} = M/I_{yy} \tag{1c}$$

$$\dot{\theta} = q \tag{1d}$$

These dynamics are reduced to a short-period model by setting V constant during any given maneuver and noting that $u = V\cos\alpha$ and $w = V\sin\alpha$. Taking derivatives of these relationships and manipulating yields

$$\dot{\alpha} = q + \frac{mg\cos\theta + Z}{mV\cos\alpha} \tag{2}$$

An algebraic expression for the thrust T is also obtained:

$$T = -X + Z\tan\alpha + mg(\sin\theta - \tan\alpha\cos\theta) \tag{3}$$

Equations (1c), (1d), (2), and (3) constitute the short-period model. The three states, α, q, and θ, are augmented by elevator dynamics,

modeled as a first-order lag with a time constant of 0.050 s. The elevator deflection is limited to ±25 deg with a slew rate limit of 60 deg/s (Ref. 16). The model was implemented using MATLAB. Tabular data from Ref. 16 for C_X, C_Z, C_M as functions of AOA and δ_e were incorporated directly into the model using custom built, two-dimensional, table-lookup functions.

IV. Conventional QFT Control Design

The objective of this control design is to allow the pilot to control AOA accurately during high-AOA maneuvers. However, before QFT is used to design the α-loop controller, a set of LTIE models must be generated and an inner q loop should be closed as will be described.

Central to this nonlinear QFT approach is the use of LTIE models. A LTIE model is a linear, time invariant model, which produces an output time history, which is an accurate reproduction of the output produced by the nonlinear aircraft model, when both are excited by the same input signal. LTIE models of the aircraft were extracted using GOLUBEV, an algorithm implemented in MATLAB by Golubev and Horowitz.[17] GOLUBEV takes the time histories of input and output signal pairs and numerically determines a transfer function relating the two. Thus, a LTIE model is not simply a linearization of the model about an equilibrium point, which is often only valid close to equilibrium. Instead, a LTIE model may represent the dynamics in a much larger region. Since the aircraft is a nonlinear system, a whole set of LTIE models is required to accurately reproduce the aircraft response for arbitrary input signals. This set serves to define the set $\mathcal{P}$. The full extent of $\mathcal{P}$ depends on the spread of the LTIE models. The number of models to include is not clear cut but should include models corresponding to the most extreme maneuvers at the most extreme parts of the operating envelope together with a cross section of points closer to nominal conditions. The number of combinations can increase rapidly when there are several independent model and input parameters to consider and so some judgement must be exercised to limit the number of model extractions necessary to realistically characterize $\mathcal{P}$.

A. Design Specifications

The design specifications are given in terms of time domain responses to certain test signals. In this case various step changes in $\alpha_{\text{stick}}(t)$ were used, for which the set of acceptable responses $\mathcal{A}$ includes first-order and moderately damped, second-order responses with less than 20% overshoot and 1-rad/s bandwidth. The upper and lower bounds on $\alpha(t)$ in $\mathcal{A}$ are shown in Fig. 3. These responses can be interpreted as bounds on the frequency response of the closed-loop transfer function between $\alpha_{\text{stick}}(t)$ and $\alpha(t)$ by taking the Laplace transforms of the bounding responses, as shown in Fig. 4.

B. Inner Loop

The F-16 has unstable short-period dynamics and so implementing an inner q loop, as in Fig. 5 before conducting the QFT design is useful. The feedback gain on q was picked by running simulations of elevator doublets of varying magnitudes. Each doublet ran for 1 s up (or down), 1 s down (or up), then 9 s off. GOLUBEV was used to extract LTIE models of the aircraft pitch response $q(t)$ vs $\delta_e(t)$, which allowed selection of a feedback gain K_q. Subsequent simulations and model extractions with the q loop closed showed that $K_q = -40$ deg/(rad/s) was a good choice, since it results in simulations that follow the inputs well and rarely lead to elevator rate limiting. The q loop remained implemented as part of the final flight control law configuration of Fig. 6. Currently, QFT is used to design the elements $C(s)$ and $F(s)$, in Fig. 6. QFT can also be used to optimize the selection of K_q, but this is not done here. The negative sign on K_q results from the sign convention on elevator deflections. Positive δ_e causes a negative pitching moment.

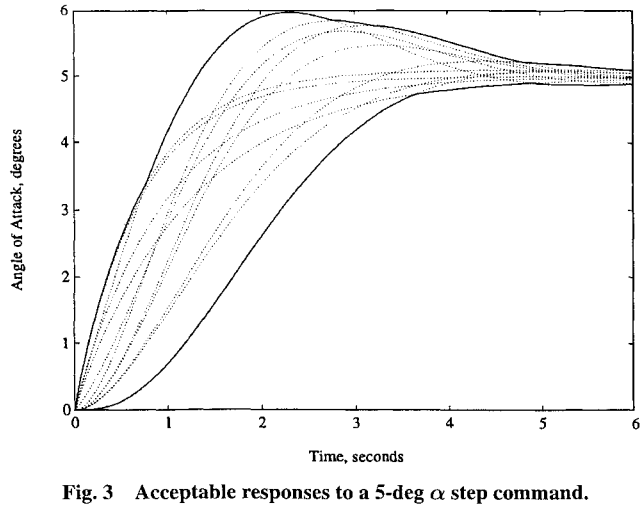

Fig. 3 Acceptable responses to a 5-deg α step command.

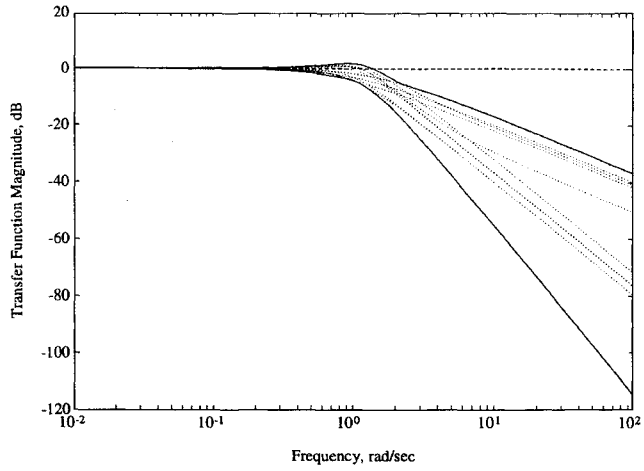

Fig. 4 Frequency domain bounds on acceptable responses.

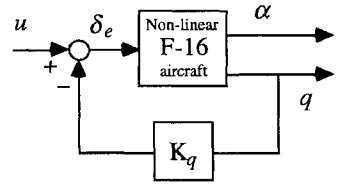

Fig. 5 Inner q loop.

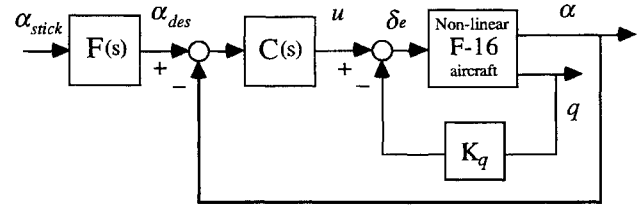

Fig. 6 AOA control configuration with q loop closed.

C. LTIE Models

The LTIE models used to design $C(s)$ and $F(s)$ represent the dynamics between $u(t)$, the input to the q loop, and the output $\alpha(t)$, in Fig. 6. These models are generated by first collecting matched pairs of output signals $\alpha(t)$ in the set $\mathcal{A}$ together with the input signals $u(t)$ required by the nonlinear model to produce those output responses. Then a LTIE transfer function is fitted to each signal pair using GOLUBEV. Computing the input $u(t)$ required to produce a desired $\alpha(t)$ response is a nontrivial task. Two basic methods are used. One is to invert the dynamic equations to determine the input signal given values of all of the states. The main disadvantages of this approach are the need to know the dynamic equations accurately and the solving of the resulting inverse equations are computationally intensive because they must be solved iteratively. The second method, favored by the authors, is to use a high-gain element $C_{\text{HG}}(s)$ in place of $C(s)$ in Fig. 6. Then a desired AOA signal $\alpha_{\text{des}}(t)$ from $\mathcal{A}$ is applied at the α loop input by using an appropriately designed prefilter $F_{\text{HG}}(s)$. The output $\alpha(t)$ should also be in $\mathcal{A}$ because the

high loop gain forces $\alpha(t)$ to track $\alpha_{\text{des}}(t)$ closely. Thus, the $u(t)$ generated within the loop can be paired with the acceptable $\alpha(t)$ response. Note that the high-gain elements, $C_{\text{HG}}(s)$ and $F_{\text{HG}}(s)$, are implemented merely to get input/output signal pairs and have nothing to do with the final flight control law, $C_{\text{QFT}}(s)$ and $F_{\text{QFT}}(s)$, which have much lower gain.

D. High-Gain Controller

$C_{\text{HG}}(s)$ is designed to yield a fast open-loop crossover frequency (>10 rad/s) to ensure that the $\alpha(t)$ closely follows the acceptable signal $\alpha_{\text{des}}(t)$. Because the relationship between $u(t)$ and $\alpha(t)$ for this aircraft model is nonminimum phase, care must be taken selecting $C_{\text{HG}}(s)$. Often different high-gain controllers are required for each group of LTIE models to guarantee stability with the high bandwidth used in the loop. Fortunately, in this case a single high-gain controller with the following transfer function sufficed for all flight conditions:

$$C_{\text{HG}}(s) = \frac{-2481(s+1)(s+10)}{s(s+50)} \tag{4}$$

Using the high-gain controller, 47 simulations of pullup and push-over maneuvers of varying severity were conducted at the flight speeds: 150, 120, 97, 78, 62, and 50 m/s. These speeds are logspaced to provide reasonable coverage of the flight envelope with a manageable number of simulations. Here, 47 different input/output pairs were generated, to which LTIE models were fitted using GOLUBEV. Although the actual aircraft has four states the best GOLUBEV fits often had other than four poles—usually five, occasionally six, and sometimes only three.

E. Templates

The magnitudes and phases of each of the 47 LTIE transfer functions were plotted on the Nichols chart at the following design frequencies: 0.125, 0.25, 0.5, 1, 2, 4, and 8 rad/s. These frequencies represent the desired closed-loop bandwidth at 1 rad/s and the primary open-loop design region three octaves above and three octaves below the expected open-loop crossover. At each frequency, templates were constructed enclosing the individual points as shown in Fig. 7. Finally, the LTIE model fitted to the 50 m/s, 6-deg pushdown simulation was selected as the template handle because it conveniently corresponds to a point near the lower left-hand corner of some templates. Note that the handle transfer function phase angle begins at -180 deg for $\omega = 0$ and decreases to -360 deg at high frequency, which again reflects the sign convention on δ_e.

F. QFT Design

After forming the templates, the boundary curves of the open-loop compensated system are computed by sweeping each template across the Nichols chart from 0 to -200 deg in 5-deg steps and moving the template vertically upward until it just fits between a pair of M curves with the allowable variation in closed-loop magnitude to be shown. The bounds shown are derived from the design

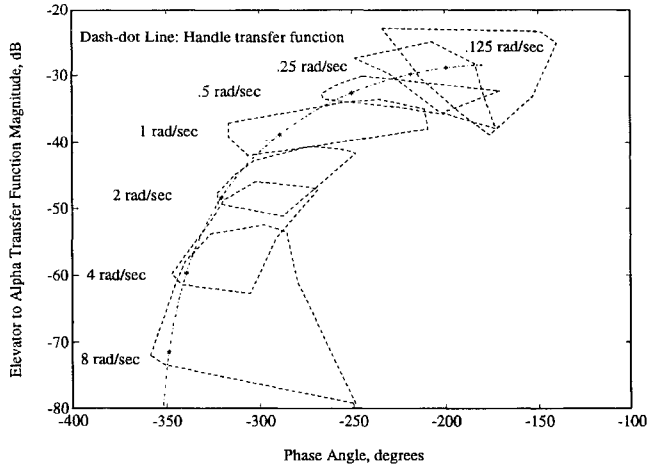

Fig. 7 Nichols chart with F-16 uncertainty templates $P(j\omega)$.

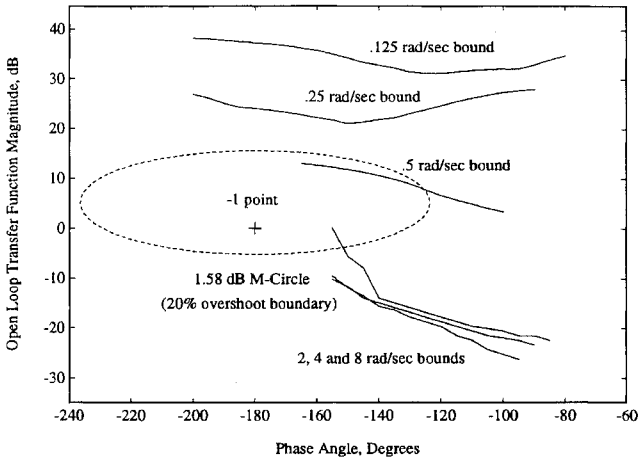

Fig. 8 QFT design bounds.

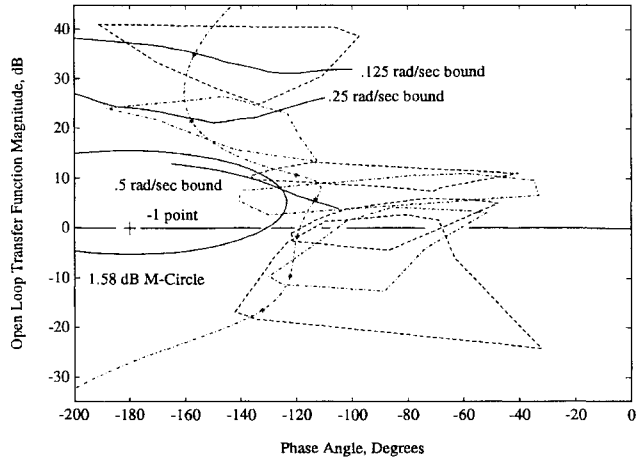

Fig. 9 QFT compensated templates $PC(j\omega)$.

specifications of earlier in the section, by computing the difference between the upper and lower bounds on the frequency response specification in Fig. 4.

The allowable M variations are 0.32, 0.76, 2.47, 5.99, 11.1, 22.3, and 34.4 dB at the respective frequencies 0.125, 0.25, 0.5, 1.0, 2.0, 4.0, and 8.0 rad/s. The loci of points swept out by the template handle as the templates traverse the Nichols chart form the performance bounds shown in Fig. 8. For an acceptable design, the handle of each template must lie above its respective bound. Also shown in Fig. 8 is the maximum allowable overshoot boundary or M-circle limit. The design meets the 20% overshoot specification if none of the templates penetrate the 1.58-dB M circle.

Designing the compensator is straightforward. A single compensator $C(s)$ is sought, which provides the gain and phase at each template frequency, to move the handle transfer function just on or above the respective performance boundary curve and so that the templates stay outside the overshoot M circle. $C(s)$ should also keep the return ratio, $P(s)C(s)$, as far to the left as possible, because, according to Horowitz,[10] doing so minimizes the magnitude of the sensor noise-to-actuator transfer function.

Figure 9 shows the result of applying compensation to the uncertainty templates. Meeting all of the QFT boundary limits was difficult. Although it was possible to keep the compensated handle transfer function above all of the closed-loop magnitude bounds, keeping all of the uncertainty templates out of the 1.58-dB overshoot M circle was impractical. Consequently, the 1 and 0.5 rad/s templates were allowed to penetrate the M-circle bound slightly, in effect trading phase margin at crossover for gain margin at high frequencies. The resulting compensator is

$$C_{\text{QFT}}(s) = \frac{-27{,}500[s^2 + 2(0.48)(0.4)s + 0.4^2](s+2.5)}{s(s+0.05)[s^2 + 2(0.7)(20)s + 20^2]} \tag{5}$$

A low-pass prefilter $F(s)$, given by Eq. (6) is required to bring the closed-loop frequency response within the specifications of Fig. 4:

$$F_{\mathrm{QFT}}(s) = \frac{(1.3)^2}{s^2 + 2(0.7)(1.3)s + (1.3)^2} \tag{6}$$

$F(s)$ places the closed-loop transfer functions of all of the models in the set $\mathcal{P}$ within the magnitude bounds of Fig. 4 up to approximately 15 rad/s (except for a small excursion near 0.4 rad/s). Beyond this, the magnitude falls below the lower bounds of Fig. 4. Reference 10 states that frequency domain bounds are not important more than one decade above the designed bandwidth of 1 rad/s and so there is no need to place a high-frequency zero in $F(s)$ to boost the closed-loop magnitudes back into the specified bounds above 10 rad/s.

V. Conventional QFT Simulations

Using the control law just described, 18 verification simulations were conducted. Pullup maneuvers of 5 and 20 deg and pushover maneuvers of 5 deg were simulated at flight speeds of 150, 120, 97, 78, 62, and 50 m/s. Overplots of the 18 simulations are shown in Fig. 10, along with the acceptable, time domain boundaries adapted from Fig. 3. All of the simulations show stable behavior and excellent command following, with the single exception of the 20-deg pullup at 50 m/s; which has an oscillatory response. The control difficulties encountered in this maneuver should come as no surprise: the initial trim AOA is 28.1 deg at 50 m/s; the AOA actually exceeds 50 deg during the maneuver.

The 5-deg pullup simulations are better behaved. All of the simulations pull in close to 5-deg AOA at the end of the 5-s α_{stick} pulse. The small excursions at 6 s may be related to the fact that the compensator does not meet all of the Nichols chart bounds as discussed in the preceding section.

The pushover maneuvers are also well behaved. All six traces fall neatly inside the time domain bounds and approach steady state by second 6, as required by the design specifications. The pushovers appear to suffer a 10% steady-state tracking error. Longer length α_{stick} pulses verify that this error decays to zero after about 10 s. The error with shorter pulses is sufficiently small to be of no particular concern in flight.

Whereas the AOA response with this control law is good, elevator response becomes noticeably oscillatory at higher speeds. Figure 11 shows that strong elevator oscillations occur following transients at 150 m/s. The oscillations appear in pitch rate and even as small ripples in AOA. Alternative controller designs showed that the oscillations could be reduced by increasing the break frequency of the rolloff poles in $C(s)$ from 20 to 40 rad/s or higher, which indicates insufficient phase margin at higher speed. Moving the rolloff poles has the adverse effect of increasing the effect of sensor noise on the elevator actuator at higher frequencies.

The elevator oscillations appearing in the 150-m/s simulations demonstrate the limitations of using a single linear compensator. To meet the tight, closed-loop magnitude specifications for such widely varying flight conditions requires high gain from $C(s)$. This

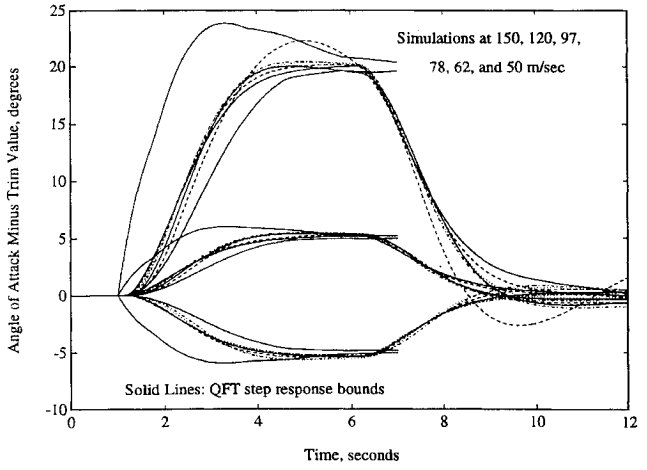

Fig. 10 Responses of $\alpha(t)$ to $\alpha_{\mathrm{stick}}(t)$ pulses.

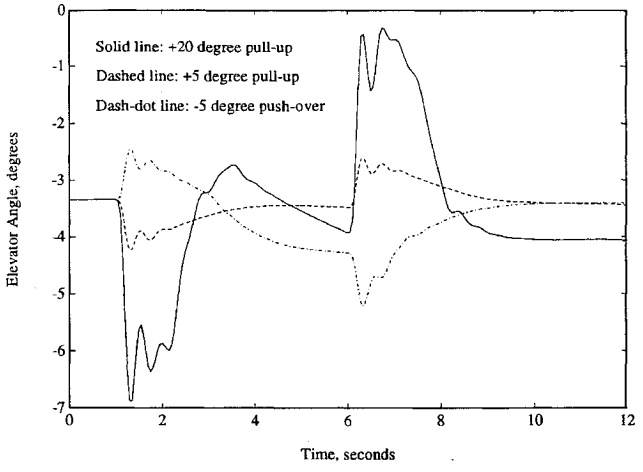

Fig. 11 Responses of $\delta_e(t)$ to $\alpha_{\mathrm{stick}}(t)$ pulses.

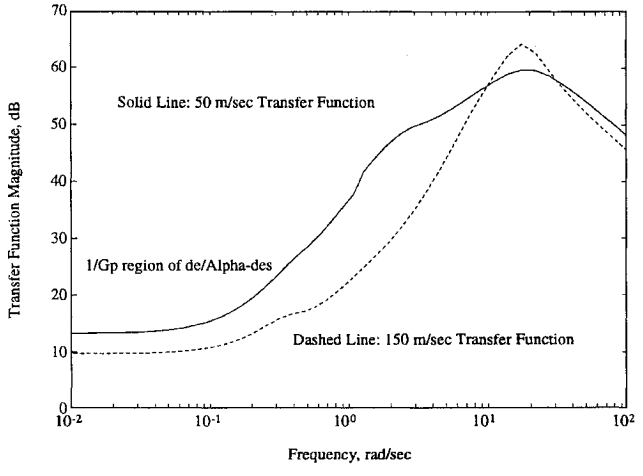

Fig. 12 Sensor noise amplification transfer function $\delta_e/\alpha_{\mathrm{des}}$.

high gain yields excessive loop gain at 150 m/s because the elevator effectiveness is nine times bigger than at 50 m/s.

LTIE models of $\delta_e/\alpha_{\mathrm{des}}$ for two representative flight conditions were extracted to produce the Bode plots in Fig. 12. Here the cause of the elevator oscillations can be explained by the narrow, lightly damped peak, seen in the plot for the 150-m/s model compared with the generally higher but flatter shape corresponding to the 50-m/s model.

VI. Gain-Scheduled Design

One way to reduce the elevator oscillations is to reduce the gain of $C(s)$ but this can only be achieved if the design specification is eased to accept larger closed-loop magnitude variation. However, by including a variable gain G_V, which decreases at higher air speeds, the increase in overall loop gain caused by increased elevator effectiveness can be canceled or reduced. Therefore, a single, scheduled gain G_V was introduced at the output of $C(s)$. G_V is inversely proportional to V. The idea is to provide sufficient gain at 50 m/s to meet the performance specification, but then reduce gain at higher speeds to avoid elevator oscillation. QFT is applied as before except that the templates are modified by the gain G_V. The new templates are obtained by simply multiplying all of the original template gains by $(V_{\min}/V)$, where $V_{\min} = 50$ m/s. The resulting reshaped templates $\boldsymbol{P}G_V$ are placed on the Nichols chart, and a new compensator design is created.

Scaling QFT templates has a cost. Whereas multiplying template gains by $(V_{\min}/V)^n$, where $n = 1, 2$, tends to make the higher frequency templates smaller, it also tends to make the lower frequency templates larger. Figure 13 shows the effect of scaling the template gains by both $(V_{\min}/V)$ and $(V_{\min}/V)^2$. The left-hand template set, shifted 40 deg to the left from its true position for clarity, is the QFT baseline template set shown earlier in Fig. 7. The center template

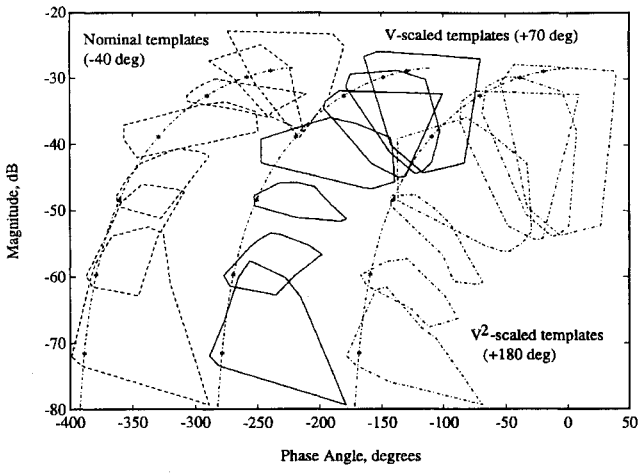

Fig. 13 V-scaled templates PG_V.

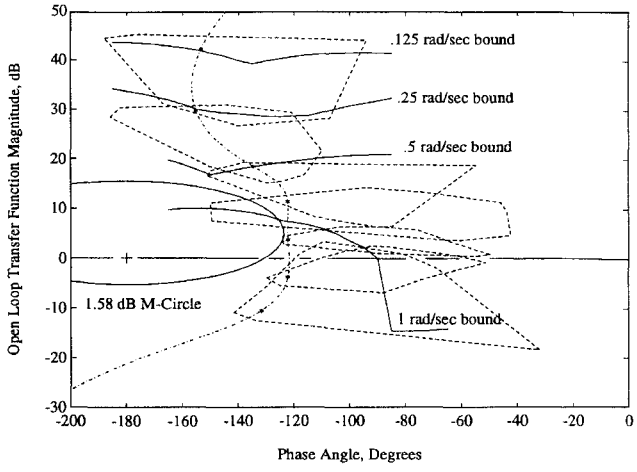

Fig. 14 V-scaled QFT compensated templates $PG_VC(j\omega)$.

set, shifted 70 deg to the right, has all gains scaled by $(V_{\min}/V)$. The rightmost set, shifted +180 deg in the plot window, scales all template gains by $(V_{\min}/V)^2$. The tradeoff between larger low-frequency templates and smaller high-frequency templates looks worthwhile for $(V_{\min}/V)$ scaling whereas the low-frequency template sizes are excessively enlarged for the $(V_{\min}/V)^2$ scaling. Consequently, only a $(V_{\min}/V)$ gain-scheduled QFT controller was designed.

Why do the templates look better when scaled by V instead of V^2? Superficially it would appear that scheduling the gain inversely with dynamic pressure $\bar{q} = \frac{1}{2}\rho V^2$ should eliminate gain variation entirely, since the control effectiveness M_{δ_e} is directly proportional to $\bar{q}$. However, consider the linearized, short-period dynamics of Eqs. (7a) and (7b),

$$\dot{\alpha} = (Z_\alpha/V)\alpha + [1 + (Z_q/V)]q + \left(Z_{\delta_e}/V\right)(u + 40q) \quad (7a)$$

$$\dot{q} = M_\alpha\alpha + M_q q + M_{\delta_e}u + 40M_{\delta_e}q \quad (7b)$$

where

$$Z_\alpha = \frac{\bar{q}SCZ_\alpha}{m}, \qquad Z_q = \frac{\bar{q}S\bar{c}CZ_q}{2mV}, \qquad \text{and} \quad Z_{\delta_e} = \frac{\bar{q}SCZ_{\delta e}}{m}$$

and

$$M_\alpha = \frac{\bar{q}S\bar{c}C_{m_\alpha}}{I_{yy}}, \qquad M_q = \frac{\bar{q}S\bar{c}^2C_{m_q}}{2VI_{yy}}, \qquad \text{and} \quad M_{\delta_e} = \frac{\bar{q}S\bar{c}C_{m\delta e}}{I_{yy}}$$

The last term in Eqs. (7a) and (7b) is the inner q-loop feedback term.

Because the Z_q and Z_{δ_e} terms in Eq. (7a) are usually small they are neglected, yielding a simplified transfer function between δ_e and α,

$$\frac{\alpha}{\delta_e} = M_{\delta_e} \Bigg/ \left[s^2 - \left(\frac{Z_\alpha}{V} + M_q + 40M_{\delta_e}\right)s + \left(\frac{Z_\alpha\left(M_q + 40M_{\delta_e}\right)}{V} - M_\alpha\right)\right] \quad (8)$$

The numerator term M_{δ_e} is proportional to $\bar{q}$. Definitions of the stability derivatives show that the coefficient of s in the denominator is directly proportional to V except for the 40 M_{δ_e} term, whereas the constant term in the denominator is proportional to V^2. Consequently, at low frequencies the open-loop gain between δ_e and α is independent of V, whereas at high frequencies the gain is proportional to V^2. Thus, G_V tends to reduce magnitude variations at higher frequencies at the expense of increased variation at low frequencies.

The scaled templates PG_V require a new set of Nichols chart boundaries. The higher frequency boundaries are lower because less gain is required to fit the smaller templates between M curves having the allowable variation. With the new boundaries, a new QFT compensator, $C_{\text{QFT}/V}(s)$, is designed to keep the position of the template handle above its respective boundaries. The locus of the return ratio, $PG_VC_{\text{QFT}/V}(j\omega)$, together with the boundaries, are shown in Fig. 14. Just as with the conventional QFT design, some of the overshoot boundaries were neglected to permit increased gain margin. The resulting compensator including G_V is

$$G_V \cdot C_{\text{QFT}/V}(s) = \frac{-55{,}000(s + 2.2)[s^2 + 2(0.65)(0.45)s + 0.45^2]}{s(s + 0.05)[s^2 + 2(0.7)20s + 20^2]}\left(\frac{50\text{ m/s}}{V}\right) \quad (9)$$

The prefilter $F_{\text{QFT}}(s)$, given by Eq. (6), worked well here for final shaping of the closed-loop magnitude.

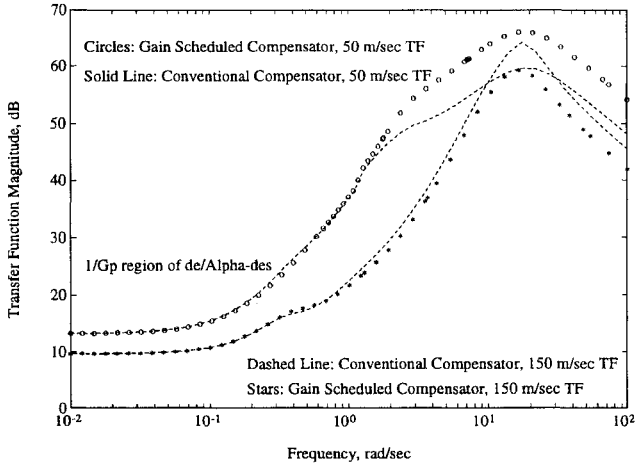

Fig. 15 Sensor noise amplification transfer function $\delta_e/\alpha_{\text{des}}$.

Figure 15 shows Bode magnitude plots of the transfer function from α_{des} to δ_e for the gain-scheduled QFT for the same two flight conditions used to make the plots of Fig. 12, which are also repeated here. Notice how the 50-m/s case involves higher gain than before, whereas the 150-m/s case is noticeably less peaky than the unscheduled design. This leads to a much improved elevator response.

VII. Gain-Scheduled Control Law Simulations

Simulations of the 18 maneuvers discussed in Sec. V were repeated here but using the gain-scheduled compensator. The results are shown in Fig. 16 and are comparable to the simulations of the conventional QFT design in Fig. 11. For 5-deg pullup commands, all six simulations approach steady state at 6 s. Two of the simulations (120 and 97 m/s) miss the tracking bounds by small margins, whereas all six simulations follow smooth paths through the transient. If anything, these simulations more nearly fill the allowable response bounds, indicating a more nearly optimal design (lower average gain) than the conventional QFT design.

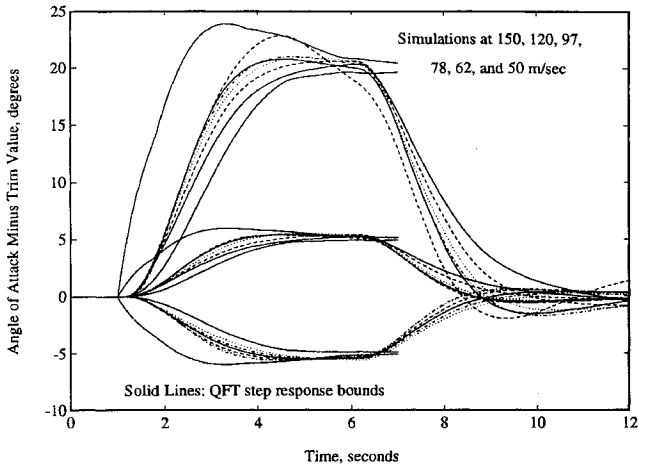

Fig. 16 Gain-scheduled $\alpha(t)$ responses to $\alpha_{\text{stick}}(t)$ pulses.

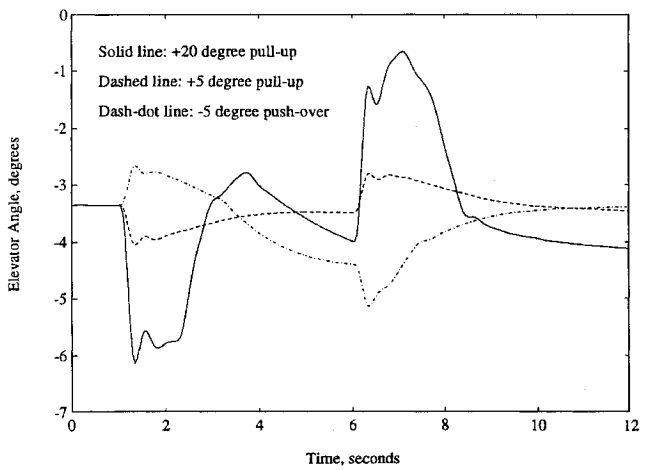

Fig. 17 Gain-scheduled $\delta_e(t)$ responses to $\alpha_{\text{stick}}(t)$ pulses.

The gain-scheduled, 20-deg pullups also look very similar to the conventional design: all simulations meet the tracking bounds at 6 s, except for the 50-m/s simulation, which overshoots as before. Again, the transient responses of the gain-scheduled compensator fill more of the allowable bounds. The 5-deg pushovers also look like the results from the conventional QFT compensator.

Both control laws are effective at controlling AOA. However, Fig. 17 shows that the gain-scheduled compensator almost completely avoids elevator oscillations, whereas the conventional design suffers up to 40% overshoots in elevator deflection following transient commands.

VIII. Conclusions

QFT provides a means to design robust compensator structures that can control systems with wide variations in physical parameters. A successful use of the technique is demonstrated. A nonlinear, short-period model of the F-16 aircraft was successfully controlled over a speed range from 50 to 150 m/s with a single compensator and prefilter. Large AOA excursions were demonstrated, including some that exceed the stall angle by nearly 40 deg. However, a single linear compensator has limitations. High loop gains, required to meet the performance objectives with the conventional QFT design, lead to excessive elevator activity. Although AOA control was excellent at all speeds, elevator oscillations appeared at higher flight speeds, causing oscillations in pitch rate and demanding high actuator rates.

The loop gain problem was attacked by inserting a gain G_V proportional to $1/V$, in series with the plant. Including this gain makes the low-frequency QFT templates larger but has the beneficial effect of making the high-frequency templates smaller. This tradeoff in template sizing pays off, because the final, QFT design has lower overall loop gain at higher speeds, which almost completely eliminates elevator oscillations.

The results of this simple, gain-scheduling idea are encouraging. Future work will investigate the use of more sophisticated nonlinear preconditioning of the plant, to reduce the template sizes further, and testing the current controller on the full, nonlinear, longitudinal model.

References

[1]Scott, W. B., "X-31 Kill Ratios Exceed Predictions," *Aviation Week and Space Technology*, Aug. 1994, pp. 54, 55.

[2]Francis, M. S., "X-31 an International Success Story," *Aerospace America*, Feb. 1995, pp. 22–32.

[3]Shamma, J. S., and Athans, M., "Gain-Scheduling: Potential Hazards and Possible Remedies," *IEEE Control Systems Magazine*, June 1992, pp. 101–107.

[4]Snell, S. A., Enns, D. F., and Garrard, W. L., "Nonlinear Inversion Flight Control for a Supermaneuverable Aircraft," *Journal of Guidance, Control, and Dynamics*, Vol. 15, No. 3, 1992, pp. 976–984.

[5]Bugajski, D. J., and Enns, D. F., "Nonlinear Control Law with Application to High Angle-of-Attack Flight," *Journal of Guidance, Control, and Dynamics*, Vol. 15, No. 3, 1992, pp. 761–767.

[6]Snell, S. A., "Preliminary Assessment of the Robustness of Dynamic Inversion Based Flight Control Laws," *Proceedings of the AIAA Guidance, Navigation, and Control Conference* (Hilton Head, SC), AIAA, Washington, DC, 1992 (AIAA Paper 92-4330).

[7]Buffington, J. M., Adams, R. J., and Banda, S. S., "Robust, Nonlinear, High Angle-of-Attack Control Design for a Supermaneuverable Vehicle," *Proceedings of the AIAA Guidance, Navigation, and Control Conference* (Monterey, CA), AIAA, Washington, DC, 1993 (AIAA Paper 93-3774).

[8]Reiner, J., Balas, G. J., and Garrard, W. L., "Robust Dynamic Inversion for Control of Highly Maneuverable Aircraft," *Journal of Guidance, Control, and Dynamics*, Vol. 18, No. 1, 1995, pp. 18–24.

[9]Horowitz, I. M., *Synthesis of Feedback Systems*, Academic, New York, 1963.

[10]Horowitz, I. M., *Quantitative Feedback Design Theory (QFT)*, Vol. 1, QFT Publications, Boulder, CO, 1993.

[11]Sating, R., Houpis, C. H., and Pacter, M., *MIMO/QFT CAD Program User's Manual*, 2nd ed., U.S. Air Force Inst. of Technology, Wright–Patterson AFB, OH, July 1993.

[12]Hess, R. A., and Gorder, P. J., "Quantitative Feedback Theory Applied to the Design of a Rotorcraft Flight Control System," *Journal of Guidance, Control, and Dynamics*, Vol. 18, No. 4, 1993, pp. 748–753.

[13]Gorder, P. J., and Hess, R. A., "Rotorcraft Flight Control System Design Including Rotor Degrees of Freedom," *Proceedings of the AIAA Guidance, Navigation, and Control Conference* (Scottsdale, AZ), AIAA, Washington, DC, 1994 (AIAA Paper 94-3692).

[14]Reynolds, O. R., Pachter, M., and Houpis, C. H., "Full Envelope Flight Control System Design Using Qualitative Feedback Theory," *Journal of Guidance, Control, and Dynamics*, Vol. 19, No. 1, 1996, pp. 23–29.

[15]Horowitz, I., "Improvement in Quantitative Nonlinear Feedback Design by Cancellation," *International Journal of Control*, Vol. 34, No. 3, 1981, pp. 547–560.

[16]Nguyen, L. T., et al., "Simulator Study of Stall/Post Stall Characteristics of a Fighter Airplane with Relaxed Longitudinal Static Stability," NASA TP 1538, Dec. 1979.

[17]Golubev, B., and Horowitz, I. M., "Plant Rational Transfer Function Approximation from Input-Output Data," *International Journal of Control*, Vol. 36, 1982, pp. 711–723.